Lean NO_x Trap Catalyst Formulation for Selective Ammonia Synthesis from Captured NO_x

Frea Van Steenweghen [a] ✉, Lander Hollevoet [a] ✉, Johan A. Martens [a] * ✉

[a] Center for Surface Chemistry & Catalysis: Characterization and Application Team (COK-KAT), Department of Microbial and Molecular Systems (M^2S), KU Leuven, 3000 Leuven, Belgium

* Corresponding author: Tel.: +3216321637; E-mail address: johan.martens@kuleuven.be

✉ frea.vansteenweghen@kuleuven.be, lander.hollevoet@kuleuven.be, johan.martens@kuleuven.be

Highlights

- NH_3 formation is strongly affected by noble metal and catalyst support formulation.
- Dry NO_x storage followed by wet reduction phase is best scenario for NH_3 formation.
- $Pt/BaO/Al_2O_3$ can achieve NH_3 formation with 82% selectivity.
- Water vapor content for optimum NH_3 formation performance of $Pt/BaO/Al_2O_3$ is 1.5%.

Abstract

In the Lean NO_x Trap (LNT) technology, ammonia (NH_3) occurs as reaction intermediate in conversion of trapped nitrogen oxides (NO_x) to nitrogen gas (N_2) using hydrogen gas (H_2) reductant. The use of an LNT for synthesizing NH_3 from NO_x is potentially an attractive option for small-scale green NH_3 production by converting locally produced NO_x pollutant to an important chemical. In this work, it is investigated to what extent the product selectivity towards NH_3 on the standard model catalyst $Pt/BaO/Al_2O_3$ can be maximized depending on reaction conditions for trapping and reducing NO_x with H_2 in the temperature range of 75-200°C. The LNT catalyst preparation was varied by using Pt, Pd and bimetallic combinations, as well as different support materials, namely Al_2O_3, TiO_2, ZrO_2 and MgO. NO_x adsorption and selectivity of captured NO_x reduction to ammonia is discussed in terms of texture and the chemical nature of the support. The NH_3 selectivity is influenced by the water vapor content in the gas feed. Storage of NO_x in absence of water followed by reduction with hydrogen gas in presence of water vapor was found to be the most favorable operation mode of the LNT for NH_3 formation. The NH_3 selectivity reached 82% at 150°C. Explanations for the role of water and in this catalytic chemistry are offered and its consequences for catalyst preparation are discussed. The optimum water content of the reacting gases is predicted to be strongly dependent on catalyst preparation.

Graphical abstract

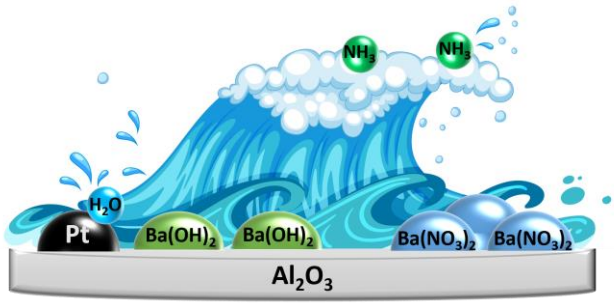

Keywords: Lean NO_x Trap, ammonia synthesis, catalyst composition, barium on alumina, water effect

1 Introduction

Lean NO_x Trap [LNT] (also known as NO_x Storage-Reduction [NSR]) is one of the technologies to eliminate nitrogen oxides (NO_x) in exhaust gases from automobile combustion engines [1,2].

In the 1990s, Toyota developed an LNT catalyst composed of a precious group metal catalyst, e.g., Pt, Rh, Pd, and a storage component, typically an alkaline-earth metal (e.g., Ba). Both components are dispersed on a metal oxide support material with large surface area, such as alumina [1,3]. The LNT operates in two alternating phases between NO_x storage and chemical reduction. In fuel-lean operating conditions, NO_x is oxidized and trapped on the alkaline Ba sites in the form of nitrites ($Ba(NO_2)_2$) and nitrates ($Ba(NO_3)_2$), of which the $Ba(NO_2)_2$ is further oxidized to the final $Ba(NO_3)_2$. This is called the NO_x storage- or adsorption phase. The LNT is regenerated in a fuel-rich gas atmosphere during which trapped NO_x species are reduced on the Pt sites to primarily nitrogen gas (N_2), but also generating ammonia (NH_3) and nitrous oxide (N_2O) as byproducts [4,5]. Among the reductants, produced in an engine running rich, carbon monoxide (CO), hydrogen gas (H_2) and unburned hydrocarbons, H_2 is most reactive. The reaction of $Ba(NO_3)_2$ with H_2 results in significant NH_3 by-product formation at low temperatures (< 250°C) [6,7]. Comprehensive reviews about LNT research have been published [8–10]. The storage and reduction mechanism with H_2 as reductant on a $Pt/BaO/Al_2O_3$ LNT is depicted by Fig. 1.

N_2 is either produced directly from nitrate reduction by H_2 (Eq. 1), or via a two-step process with NH_3 intermediate. In case of the latter, the first step is a fast reduction of stored nitrates with H_2 to form NH_3 (Eq. 2) [11]. While in the second step, NH_3 itself acts as reductant and reacts with the still-stored nitrates to N_2 (Eq. 3) [7,12]. Considering that NH_3 is a less reactive reductant than H_2, this second reaction is slow and rate-determining in the formation of N_2 [4].

$$Ba(NO_3)_2 + 5\,H_2 \rightarrow N_2 + BaO + 5\,H_2O \quad (1)$$
$$Ba(NO_3)_2 + 8\,H_2 \rightarrow 2\,NH_3 + BaO + 5\,H_2O \quad (2)$$
$$3\,Ba(NO_3)_2 + 10\,NH_3 \rightarrow 8\,N_2 + 3\,BaO + 15\,H_2 \quad (3)$$
$$Ba(NO_3)_2 + 4\,H_2 \rightarrow N_2O + BaO + 4\,H_2O \quad (4)$$

The primary objective of LNT technology in the automotive applications is to cut down NO_x emissions from combustion engines in order to comply with the stringent regulatory standards for pollutant emissions. Therefore, the LNT was formerly designed to attain maximum selectivity towards N_2 and to avoid the formation of NH_3 (Eq. 2) and N_2O (Eq. 4), because of the deleterious impact on environment and human health, as well as the greenhouse gas effect, respectively [13,14].

The formation of ammonia by-product on an LNT has inspired the combination of an LNT unit with a Selective Catalytic Reduction (SCR) unit in exhaust purification systems, known as LNT-SCR [3,15]. SCR has been applied in stationary combustion engines since the 1970s and is based on the chemical reduction of NO_x to N_2 by NH_3 as reductant. The main drawback of SCR is the injection of the external reducing agent [16]. In the concept of LNT-SCR, NH_3 formed on the LNT, is used as reducing agent in the subsequent SCR system [14,17]. LNT-SCR is able to achieve higher NO_x conversion and N_2 selectivity to comply with increasingly challenging emission legislation [18,19].

The latest potential application of LNT is the small-scale production of green NH_3 from NO_x emissions. In this case, NH_3 formation needs to be maximized instead of minimized since the alternative reduction of stored NO_x to N_2 represents a loss of reagents [20,21]. Research towards maximizing NH_3 formation on an LNT in view of coupling with SCR or for small-scale green NH_3 production resulted in NH_3 selectivity's of 75-90% at relative low temperatures (< 175°C) [5,17,21–24].

Pt, Pd, and Rh, play a key role in the LNT mechanism, as they accelerate the NO oxidation reaction under lean conditions, as well as the nitrate reduction under rich conditions [9]. Furthermore, literature agrees that the support material influences catalyst activity, and more specifically product selectivity [25–27]. Deposition of the noble metal on the support is to be preferred over the barium phase to prevent agglomeration and ensure high dispersion of the noble metal. Available literature provides little information on catalyst preparation aspects for maximal NH_3 yields on an LNT.

Furthermore, literature provides limited insights into dealing with water vapor levels in the feed, particularly when they deviate from those typically encountered in automotive applications with internal combustion engines. For instance, in diesel engine exhaust the H_2O concentration can go up to 12% [28]. While water is always present in the automotive pollution control application of an LNT, in ammonia synthesis application it can be added or left out of the gas composition in either the NO_x adsorption or nitrate reduction step. There is general consensus that water enhances NH_3 formation in nitrate reduction step [4,29,30]. In this work, the H_2O presence in the gas feed of the two phases, as well as the concentration of water vapor in the gas feed, was altered to search for optimization and deeper understanding of underlying molecular mechanisms.

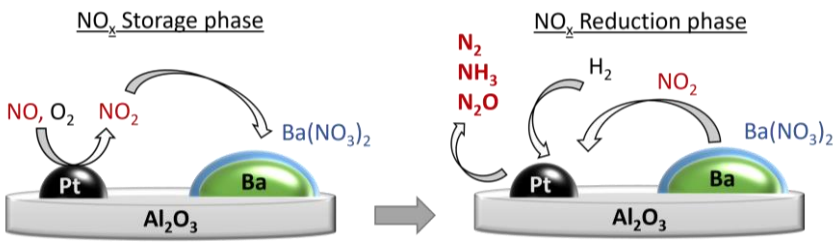

Fig. 1: Illustration of the NO_x storage/reduction mechanism of the model $Pt/BaO/Al_2O_3$ catalyst.

2 Material & Methods

2.1 Catalyst preparation

Pt/BaO/γ-Al_2O_3 catalyst with nominal weight ratio of 1/20/100, often used in literature [31,32], was prepared as follows. First, pellets of γ-alumina (Alfa Aesar, 99.97%) were crushed and sieved to obtain particle size of 125-250 µm. This particle fraction was calcined for 5 h in air at 550°C. Pt was loaded before BaO to ensure a good dispersion of the noble metal on the support material [4]. Pt was introduced through incipient wetness impregnation (IWI) with an aqueous solution of chloroplatinic acid (Merck, 99.95%) to obtain a weight-based loading of 1/100 Pt/Al_2O_3. The Pt precursor mass was calculated as 1 wt% of the support mass by taking into account the molecular weights of Pt and its precursor. The amount of aqueous solution was set to 1 mL for 1 gram of sample. Therefore, the required amount of water was found by subtracting the total volume of solution minus the Pt precursor volume. Drying was carried out at room temperature for 1 h and at 60°C for 1 h. Finally, the powder sample was calcined for 5 h at 550°C with a heating rate of 1°C.min^{-1} from room temperature. The BaO loading of Pt/Al_2O_3 was done using an aqueous solution of barium acetate (Merck, 99%). The BaO precursor mass was calculated as 20 wt% of the obtained Pt/Al_2O_3 mass by taking into account the molecular weights of BaO and the precursor. The volumes were calculated like for Pt loading. The followed drying and calcination steps were the same as for the Pt loading. Finally, the sample was cooled and sieved again. The particle fraction of 125-250 µm was retained as catalyst granules to be loaded in a tubular reactor with internal diameter of 4 mm for optimal plug flow [21].

Following the same preparation procedure, other LNT catalyst compositions were prepared using palladium(II) nitrate hydrate (Acros, > 95%), and TiO_2 (CrystalACTIV, 99%), ZrO_2 (Nikkato corporation, 95%), and MgO (Merck, extra pure) support materials. The sample notation refers to the weight ratios of noble metal to barium to alumina. For instance, Pt/BaO/Al_2O_3 (1/20/100) is a catalyst with weight ratios of 1 to 20 to 100 for Pt, BaO and alumina, respectively.

2.2 Catalyst characterization

High-Resolution Scanning Electron Microscopy (HR-SEM) was performed with a Nova NanoSEM 450 microscope (FEI, Holsboro, OR). The non-conductive powder samples were dispersed on a carbon tape and, as will be indicated, coated with carbon. The prepared samples were investigated using the indicated electron beam and stage bias. In Fig. 2A, the Ba content is visible as white structures, while in Fig. 2B the two white dots represent Pt particles. Fig. 2C depicts both the white structures and dots representing Ba and Pt, respectively.

The texture of support materials and catalyst samples was investigated using nitrogen physisorption experiments on a Quantachrome Autosorb-iQ instrument at 77K. The specific surface areas were estimated using the Brunauer-Emmett-Teller (BET) method. Pore volumes were estimated using t-plots. For the mesoporous supports, the average pore size was estimated using the density functional theory (DFT) method. Isotherms and pore size distributions can be found in Supplementary information (SI), Section 1.

The actual Pt and Ba content of catalyst samples were confirmed by chemical analysis of dissolved samples by Inductive Coupled Plasma Optical Emission Spectroscopy (ICP-OES) on a Varian 720-ES instrument. Digestion of the powder was achieved by HF treatment: 50 mg sample with 0.5 mL *aqua regia* (3:1 HCl:HNO_3) and 1.5 mL HF (40%) in a Teflon beaker for 1 h at 150°C on a stirring plate. The sample was then transferred to a 100 mL plastic flask. An amount of 1.5 g H_3BO_3 was added, followed by dropwise dilution with water. The ICP data can be found in SI, Section 2.

2.3 Catalytic experiments

A quartz tube (inner diameter: 4 mm, length: 15 cm) was loaded with 60 mg of catalyst sample, supported by quartz wool. The sample tube was placed vertically into an automated continuous flow fixed bed microreactor with online reaction product analysis. The outlet gas concentrations of NO, NO_2 and NH_3 were measured by an ABB AO2020-Limas11HW UV photometer, while the N_2O concentration was measured by an ABB AO2020-URAS26 NDIR photometer. The local catalyst temperature was measured by a fine thermocouple, immersed into the catalyst bed [33].

Gases were supplied by Air Liquide with following purities: N_2 ≥99.999%, O_2 ≥99.5%, NO (5% in He) ≥99.999%, H_2 ≥99.999%, and their delivery controlled by Mass Flow Controllers (MFC). Gases were premixed in two separated channels: one for the storage phase gases, namely NO, O_2 in N_2 carrier gas, and one for the reductant H_2 in N_2 carrier gas. A pneumatically operated 4-way valve was used to alternate between these two gas channels [34]. In both channels, N_2 gas passed through an H_2O saturator, which generates a water-saturated gas mixture with a water content depending on saturation temperature. The outlet gases were diluted with an N_2 purge to shift the gas concentrations within detectable limits of the detectors [33].

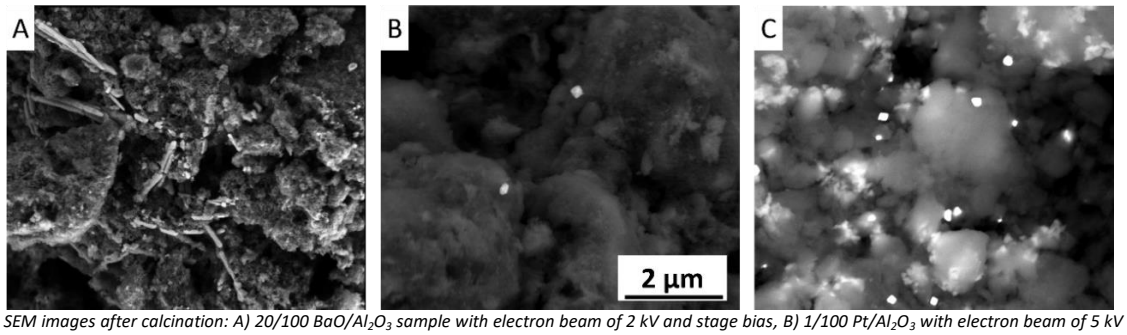

Fig. 2: SEM images after calcination: A) 20/100 BaO/Al_2O_3 sample with electron beam of 2 kV and stage bias, B) 1/100 Pt/Al_2O_3 with electron beam of 5 kV and stage bias, and C) carbon-coated 1/20/100 $Pt/BaO/Al_2O_3$ with an electron beam of 15 kV. The scale of 2 µm applies to all three images.

The standard experiment protocol consisted of three cycles of successive storage and reduction phases. The standard activity test comprised the following operating conditions. In the storage phase, a gas mixture of 200 ppm NO, 5% O_2 and 4.2% H_2O in an N_2 carrier gas was sent over the LNT catalyst during a storage time of 250 s. These NO, O_2 and H_2O concentrations represent a typical average exhaust gas derived from combustion processes [35]. Typical ranges are: 100-1000 ppm for NO with 200 ppm as most prominent [35–37], 0.5-15% for O_2 [28,35,38] and 1-20% for H_2O [28,39]. During the reduction phase with a duration of 1,800 s, the trapped NO_x was reduced by 5% H_2 [40] in N_2 carrier gas with 4.2% H_2O. The gas hourly space velocity (GHSV) was set at 60,000 h^{-1} by fixing the total gas flow rate at 6 $L.h^{-1}$ [41]. The investigated temperature range was 75-200°C with downwards steps of 25°C and with a cooling rate of 10 $°C.min^{-1}$.

For tests without H_2O in one of the phases or both phases, one or both H_2O saturators were bypassed. The temperature of the H_2O saturators was altered in the range from 5°C to 55°C, to obtain different water vapor concentrations in gas feed, going from 0.6% to 14%, according to the Antoine equation [42]. The natural temperature around the saturator is invariably ca. 29°C, generating the standard water content of 4.2% in the gas feed.

Temperature programmed desorption (TPD) tests were performed using the reactor. For this, the standard experimental protocol was extended with an additional heating phase after the storage and reduction phase. During this TPD phase, the temperature was increased to 450°C at a heating rate of $15°C.min^{-1}$ and with a holding time of 600 s in a pure N_2 gas or an H_2/N_2 gas with 5% H_2.

Prior to each experimental run, the catalyst sample underwent a preconditioning at 350°C with three cycles of storage phase (250 s) in a gas flow of 1,000 ppm NO, 5% O_2, 4.2% H_2O in an N_2 carrier gas, and reduction phase (1,800 s) with 5% H_2 in N_2 carrier gas [33]. This pretreatment aims to remove remaining adsorbed N-species of previous runs. In this way, reproducible data were obtained on preconditioned catalysts. An experimental run began with a bypass phase, in which three NO pulses were directly sent to the detector, bypassing the reactor.

2.4 Data processing

Careful calibration of the detectors was needed to obtain accurate mass balances. The exact amount of NO fed to the reactor (NO_{in}) was calculated as average of the three NO pulses directly sent to the detectors during bypass phase. NO fed to the reactor was leaving the reactor unchanged (NO_{out}) or converted to NO_2 ($NO_{2,out}$), or being adsorbed. The detector measured the gas fractions y_i of the species in the outlet, which could be converted to the molar flow rate $\dot{n}_i$ by Eq. 5. The NO_x storage efficiency and the NH_3 selectivity were the key parameters in this study. The NO_x storage efficiency [%], meaning the adsorbed fraction of NO_{in}, was calculated in Eq. 6 [5].

$$\dot{n}_{i,out} = y_{i,out} \frac{\dot{v}_{tot}}{22.4\ L\ mol^{-1}} \quad (5)$$

$$NO_x\ Storage\ eff. = \frac{\int_0^{t_{stor}} (\dot{n}_{NOin} - \dot{n}_{NO,out} - \dot{n}_{NO2,out}) dt}{\int_0^{t_{stor}} \dot{n}_{NOin} dt} \quad (6)$$

With $\dot{n}_i$ the molar flow rate [$mol.s^{-1}$], y_i the gas fraction of species i, , $\dot{v}_{tot}$ total gas flow rate [$L.s^{-1}$], 22.4 $L.mol^{-1}$ the molar volume of an ideal gas, and t_{stor} the storage phase time [s].

The amount of NH_3 formed during reduction ($\dot{n}_{NH3,out}$) was measured with Eq. 5, leading to the calculation of the NH_3 selectivity (S_{NH3}) averaged over the reduction phase using Eq. 7.

$$S_{NH3} = \frac{\int_{t_{0,red}}^{t_{end,red}} \dot{n}_{NH3,out} dt}{n_{NOadsorbed}} \quad (7)$$

The NH_3 peak concentration was found as the maximum height of the outlet NH_3 concentration during reduction. The NH_3 half peak width was determined as the reduction duration at which the detector registered 50% of the NH_3 outlet.

3 Results & discussion

3.1 Investigation of LNT catalyst composition for NH_3 synthesis

3.1.1 Noble metal function

Pt is most commonly used in LNT catalysts and is known for its excellent oxidation activity, whereas Pd and Rh exhibit high reduction activity of nitrates [8]. Due to the findings presented by Breen *et al.* [43] which demonstrate that Pt and Pd outperform Rh in NH_3

formation, Rh was excluded from experimental evaluation in this study. The use of Pd instead of Pt has been investigated based on its good reputation in Three-Way catalysts. Even higher NO_x storage capacity and reduction efficiency was found for Pd compared to Pt in the LNT application [44,45]. Furthermore, Liu & Gao [9] suggested the bimetallic combination of both would achieve higher overall NO_x conversion.

Four different precious metal catalysts were investigated, namely 1 wt% Pt, 1 wt% Pd, 1/1 wt% Pt/Pd, and 0.5/0.5 wt% Pt/Pd, all with the same BaO/Al_2O_3 weight ratio of 20/100. The $Pt/Ba/Al_2O_3$ (1/20/100) sample was prepared two times to verify the repeatability of the catalyst preparation, which was found to be satisfactory (Fig. 3). In Fig. 3A, the NO_x storage performance of the different samples at different temperatures is presented. At temperatures > 125°C, all NO_x can be stored, aligning with literature findings which have revealed that in the applied temperature range kinetic limitations hold for NO_x storage [46]. At temperatures ≤ 125°C, the NO_x storage performance depends on the catalyst composition and the noble metal loading. A higher noble metal content is accompanied by a higher storage efficiency, as can be seen in Fig. 3A where the 1/1 Pt/Pd has the highest NO_x storage efficiency. For the same noble metal content, Pt exhibits higher storage efficiency than Pd and is therefore considered a better NO_x oxidation catalyst, in agreement with literature [8,9].

Fig. 3B compares the NH_3 selectivity of the samples as depending on temperature. The existence of an optimum temperature can be explained by difficult desorption of NH_3 at low temperatures, and consecutive reaction of NH_3 towards N_2 at higher temperature. In the lower temperature range (< 150°C), Pt is significantly better than Pd with an NH_3 selectivity of 63% at 100°C. The two bimetallic systems show intermediate NH_3 selectivity's of 46% for 0.5/0.5 and 49% for 1/1 Pt/Pd. The Pd catalyst is least effective for forming NH_3, with 36% selectivity at 100°C. These results indicate that below 150°C the presence of Pd lowers the formation of NH_3 by promoting reduction towards N_2. However, at higher temperatures (≥ 150°C) the single-Pd sample achieves higher NH_3 selectivity (48% at 175°C) than the Pt sample (42% at 175°C). In this temperature region, the 0.5/0.5 Pt/Pd formulation is the best performing catalyst with NH_3 selectivity of 52% at 175°C, achieving optimal synergy between Pt and Pd. The catalysts with the lowest NH_3 selectivity appear to be the 1 Pt and 1/1 Pt/Pd. These results suggest a larger content of Pt accelerates the consecutive reaction towards N_2 above 150°C. To summarize, Pt emerges as a more proficient catalyst compared to Pd in attaining selective NH_3 formation in the lower temperature range of 100-125°C envisioned for an ammonia synthesis process consuming least energy. Operation at higher temperature would make Pd a more favorable choice.

3.1.2 Support material function

The support material was varied next. Literature stated that the NO conversion and product selectivity are highly support dependent [25,26]. γ-Al_2O_3 is generally applied as support material due to its desirable textural properties and its acid-base characteristics [47]. Furthermore, alumina can serve as storage component for NO_x by the formation of some Al-nitrate [48]. However, this storage capacity is negligible compared to the storage capacity of the Ba sites [9,49]. Nevertheless, other support candidates, namely titania (TiO_2), zirconia (ZrO_2) and magnesia (MgO) have been cited by Roy & Baiker [8] as promising support materials for the LNT catalyst [27]. TiO_2 is recently reported as catalyst for electrocatalytic reduction of NO_x towards NH_3 by Chen *et al.* [50].

Specific surface area and porosity data obtained with N_2 physisorption of support materials and catalyst samples are presented in Table 1. Nitrogen adsorption isotherms and pore size distribution can be found in SI, Section 1. SEM images of the four supports loaded by Pt and Ba can be found in SI, Section 3.

The γ-Al_2O_3 support has a BET surface area and pore volume of 280 $m^2.g^{-1}$ and of 0.859 cm^3/g, respectively. In Table 1, surface area and pore volume are expressed in two ways, based on catalyst weight and weight of support alone, respectively. Barium loading decreases the surface area as well as pore volume of $Pt/BaO/Al_2O_3$ catalyst. Assuming that the BaO does not contribute to surface area, the loading of barium decreases the surface area from 280 to 226 $m^2.g_{support}^{-1}$. The pore volume decreases from 0.859 $cm^3.g_{support}^{-1}$ to 0.669 $cm^3.g_{support}^{-1}$. Revealing the effective use of the support for spreading the barium. The mean pore size increases from 9.4 to 11.3 nm. This is tentatively explained by preferential filling of the smallest mesopores with barium.

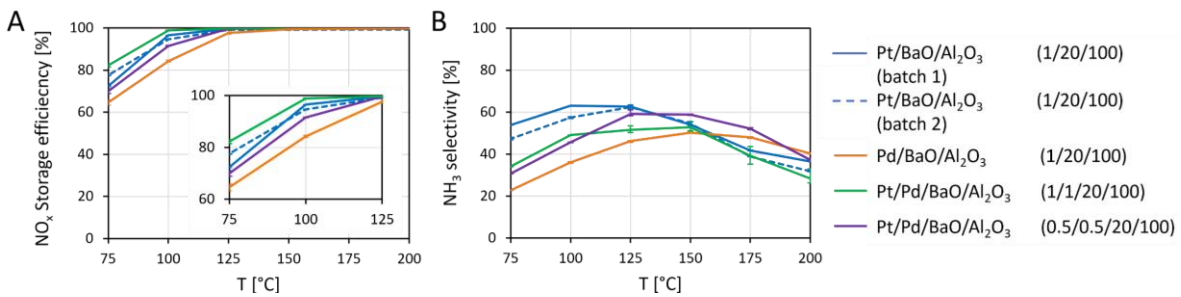

Fig. 3: A) NO_x storage efficiency [%] during the storage phase of the cycle and B) NH_3 selectivity [%] averaged over the reduction phase of the cycle of four catalysts: $Pt/BaO/Al_2O_3$ (1/20/100) (batches 1 and 2), $Pd/BaO/Al_2O_3$ (1/20/100), $Pt/Pd/BaO/Al_2O_3$ (1/1/20/100) and (0.5/0.5/20/100) against temperature in the range of 75-200°C, tested for three cycles of storage/reduction with an N_2 flush (N) between each phase (250 s S/120 s N/1800 s R/120 s N) at a GHSV of 60,000 h^{-1}. Error bars represent standard deviations.

Table 1: BET surface area S_{BET} [$m^2.g^{-1}_{support}$], total pore volume V_{pore} [$cm^3.g^{-1}_{support}$] and average pore size d_{pore} [nm] for support materials and catalyst samples

	S_{BET}		V_{pore}		d_{pore}
	$m^2.g^{-1}_{cata}$	$m^2.g^{-1}_{support}$	$cm^3.g^{-1}_{cata}$	$cm^3.g^{-1}_{support}$	Nm
Al_2O_3	280		0.859		9.4
$Pt/BaO/Al_2O_3$ (1/20/100)	192	226	0.563	0.669	11.3
TiO_2	78		0.264		13
$Pt/BaO/TiO_2$ (1/20/100)	52	63	0.187	0.220	13
MgO	45		0.210		3.9
Pt/BaO/MgO (1/20/100)	38	45	0.230	0.273	25
ZrO_2	< 10		/		/

TiO_2 support has anatase structure and consists of individual small particles, the stapling of which gives rise to mesopores. Magnesia has similar features. For the titania support, similar observations were made as for alumina concerning the changes of surface area and porosity after metal loading, confirming the effective use of the support material. The specific surface area of magnesia did not change after metal loading, suggesting the support was less efficiently used. In addition, the mean pore size increases notably implicating the metal loading had reordered the small support particles. The zirconia support had exceedingly small specific surface area.

NO_x storage efficiencies and ammonia selectivity's of catalysts with alumina, titania, magnesia and zirconia support are presented in Fig. 4. Two alumina catalysts were evaluated, viz. $Pt/BaO/Al_2O_3$ (1/20/100) and (1/20/77) (Fig. 4A and B). The NO_x storage efficiency and NH_3 selectivity were remarkably similar. At 125°C and higher temperatures, all NO_x from the feed was adsorbed. For the 1/20/100-composition under such circumstances ca. 5.1 10^{-5} mol NO_x is stored per gram catalyst. Considering $Ba(NO_3)_2$ to be formed, ca. 2.6% of the Ba atoms is involved. Ba is a heavy chemical element. The Ba content of the catalyst is such that the alumina support provides that much surface area and porosity that the amount of support can be lowered without affecting the performance. The NH_3 selectivity's of the two alumina-supported samples are at 150°C of 67% and 70%, respectively.

Titania-supported catalyst was prepared with two compositions differing in support content. With titania catalyst NO_x was less efficiently captured (Fig.4C). The specific surface area of this support (78 $m^2.g^{-1}$) is substantially lower than for the alumina. The presence of more TiO_2 support in the catalyst formulation makes NO_x trapping worse. The higher support amount could mean better spreading of barium, but also less amount of platinum and barium present as catalyst in the reactor. The ammonia selectivity is quite low on TiO_2-supported catalyst (Fig.4D). The poor selectivity is tentatively ascribed to less efficient use of the platinum which could be buried under the barium phase deposited after the platinum. Adding more support improves the ammonia selectivity a little because of the less buried and more accessible Pt sites.

Magnesia has still smaller specific surface area of 45 $m^2.g^{-1}$. The NO_x trapping efficiency was also lower than on the alumina catalysts. Here also holds higher amount of support decreases the NO_x trapping efficiency for the same reason as for TiO_2. The ammonia selectivity was better than on TiO_2, which could be tentatively explained by the platina being less covered by barium. The specific surface area of the formulation with MgO not changing upon barium loading (45 $m^2.g_{support}^{-1}$) hints at such speculative interpretation.

The zirconia formulation with incredibly low specific surface area and strong aggregation of the barium is trapping the NO_x with limited efficiency. Moreover, it has low ammonia selectivity.

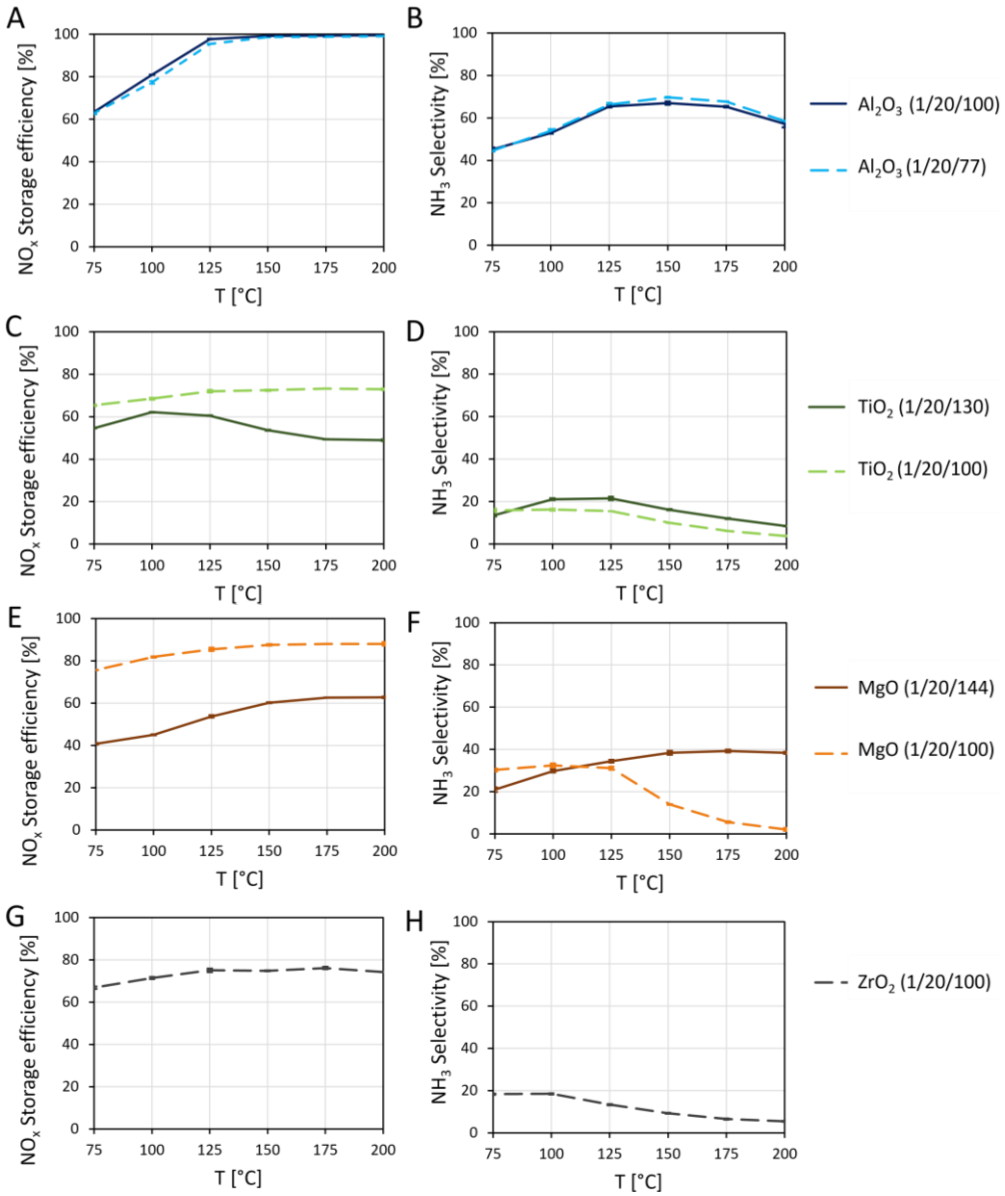

Fig. 4: NO_x storage efficiency [%] during the storage phase of the cycle (A, C, E, and G) and NH_3 selectivity [%] averaged over the reduction phase of the cycle (B, D, F, and H) in function of temperature (75-200 °C) for catalysts with different support materials: A and B, Al_2O_3 (Pt/BaO/Al_2O_3 1/20/100) and (Pt/BaO/Al_2O_3 1/20/77); C and D, TiO_2 (Pt/BaO/TiO_2 1/20/100) and (Pt/BaO/TiO_2 1/20/130); E and F, MgO (Pt/BaO/MgO 1/20/100) and Pt/BaO/MgO 1/20/144); and G and H, ZrO_2 (Pt/BaO/ZrO_2 1/20/100), tested for three cycles of storage/reduction (250 s S/1800 s R) at a GHSV of 60,000 h^{-1}. Error bars represent standard deviations.

3.2 Water influence on storage and chemical reduction of stored NO_x

To uncover the effect of water and its possible impact on catalyst design, additional experimental tests were set up with the best performing model catalyst Pt/BaO/Al_2O_3 1/20/100 (Table 2): (I) a standard experiment with 4.2% H_2O vapor present during NO_x storage as well as reduction phase, (II) an experiment in absence of H_2O vapor during storage phase and 4.2% H_2O vapor during reduction phase, (III) an experiment with 4.2% H_2O vapor during storage phase and no H_2O vapor during the reduction phase, (IV) an experiment without H_2O vapor during both phases.

Table 2: Four experiments on Pt/BaO/Al_2O_3 (1/20/100) with water vapor present or absent during NO_x storage and reduction phase

Case	Water present during storage phase (S)	Water present during reduction phase (R)
(I)	Yes	Yes
(II)	No	Yes
(III)	Yes	No
(IV)	No	No

3.2.1 Water influence on NO_x trapping

The impact of H_2O on the NO_x storage mechanism has already been discussed in literature. Lietti *et al.* [32] revealed competitive adsorption of H_2O and NO_x on the storage Ba sites. NO_x storage is accompanied by release of H_2O [49,51]. This molecular process can be seen as ligand exchange on the Ba sites between hydroxyl- and nitrate ligands. Hydroxylation of the barium oxide surface is opening up the adsorbent structure, facilitating the penetration and reaction of NO_x molecules. Moreover, literature confirms the actual presence of barium hydroxide hydrate ($Ba(OH)_2.2H_2O$) at the investigated temperature range [52]. At low temperatures (< 250°C), H_2O molecules promote nitrite formation, as it facilitates NO_x transfer towards the Ba sites, while it does not promote the subsequent oxidation to nitrate species [29,53,54]. Another effect, proposed by Szanyi *et al.* [55], is the reversible morphology change of the Ba phase, in the presence of H_2O, from a highly dispersed phase on the support, to larger bulk-like Ba agglomerates, more segregated on the support [56,57].

The NO_x storage efficiency in the temperature range of 75-200°C for the different Cases with water vapor present or absent during storage and reduction phases (Table 2) is presented in Fig. 5. Chemical reaction is expected to be accelerated by increasing temperature, as observed experimentally (Fig. 5).

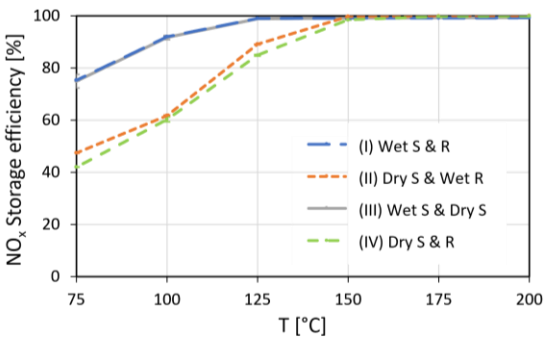

Fig. 5: NO_x storage efficiency [%] during the storage phase of the cycle at temperatures in the range of 75-200°C for Cases (I)-(IV) of Table 2. Three storage (S) and reduction (R) (250 s S/1800 s R) cycles performed at each temperature at a GHSV of 60,000 h^{-1}. Error bars represent standard deviations.

Under the investigated experimental conditions, the H_2O effect is of importance only at temperatures below 150°C. At higher temperatures, the adsorbent eliminated all NO_x from the gas fed to it. In the temperature range 75-150°C, the highest NO_x storage efficiency is reached with water present during NO_x storage (Cases (I) and (III)). The difference between Case (I) and Case (III) is the presence or absence of water during the reduction phase. This difference does not lead to a difference in NO_x adsorption behavior in a series of three consecutive storage-reduction cycles. H_2O molecules have a positive impact during the NO_x storage phase only. In Cases (II) and (IV) in which no H_2O is present during storage phase the NO_x storage efficiency is significantly lower. Also, for these two Cases, the presence or absence of water during the reduction of the adsorbed NO_x has no influence on the next storage phase.

The observed beneficial effect of H_2O on the storage mechanism can potentially be linked to the formation of bulk $Ba(NO_3)_2$ particles. Szanyi *et al.* [55] revealed that water facilitates the conversion of dispersed surface $Ba(NO_3)_2$ presence in a monolayer on the alumina surface into larger $Ba(NO_3)_2$ particles. This change in morphology of the NO_x storage phase is reversible and enhances the uptake of NO_x species. This phenomenon is confirmed in this work by SEM images (Fig. 6). Fig. 6A shows the $Pt/BaO/Al_2O_3$ sample after a long NO_x storage phase of 6,000 s in absence of water vapor, while Fig. 6B shows the same sample after a long NO_x storage phase in presence of water vapor. SEM images reveal clear differences highlighting the impact of H_2O. The white dots on Fig. 6A visualize Pt particles, and the greyish large bulk features the alumina support covered with a layer of dispersed $Ba(NO_3)_2$. In Fig. 6B, dendritic, flaky, white structures are visible on the alumina surface, which are too abundant for being due to Pt, and which can be assigned to the agglomerated $Ba(NO_3)_2$ particles.

The storage mechanisms in the dry and wet case are sketched in Fig. 7. The redox chemistry on the Pt function has been omitted. The scheme departs from the formation of nitrate ligands on a first Ba site. Barium is presented as BaO in absence of water (Fig. 7 above) , and as $Ba(OH)_2$ in presence of water (Fig. 7 below), both covering the alumina support surface. The nitrate formation propagates with the conversion of "NO_2" molecules towards nitrate ligands instead of oxide ligands in the scheme above, while instead of hydroxyl ligands in the scheme below [32]. In both cases, the next step is nitrate migration by ligand exchange. $Ba(NO_3)_2$ formed in presence of water is mobile. It migrates over the alumina surface and agglomerates. This agglomeration phenomenon does not happen in the dry case. These differences lead to a distinct situation at the end of the NO_x storage phase, which is visible on the SEM images (Fig. 7). The impact of these different situations at the start of the reduction phase is discussed in the next section.

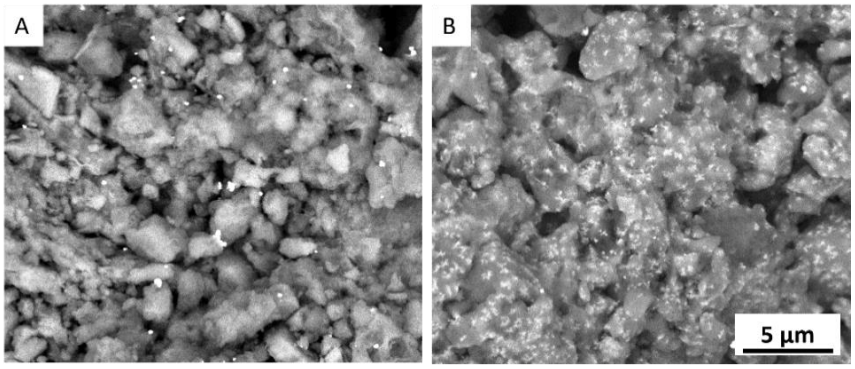

Fig. 6: SEM images of Pt/BaO/Al_2O_3 samples after long storage phase (6,000 s) of 200 ppm NO, 5% O_2 in N_2 carrier gas at 125°C. A) Dry case, B) Wet case with 4.2% H_2O in gas flow. Both images taken with electron beam of 5 kV and stage bias of 4 kV. The scale of 5 µm applies to both figures.

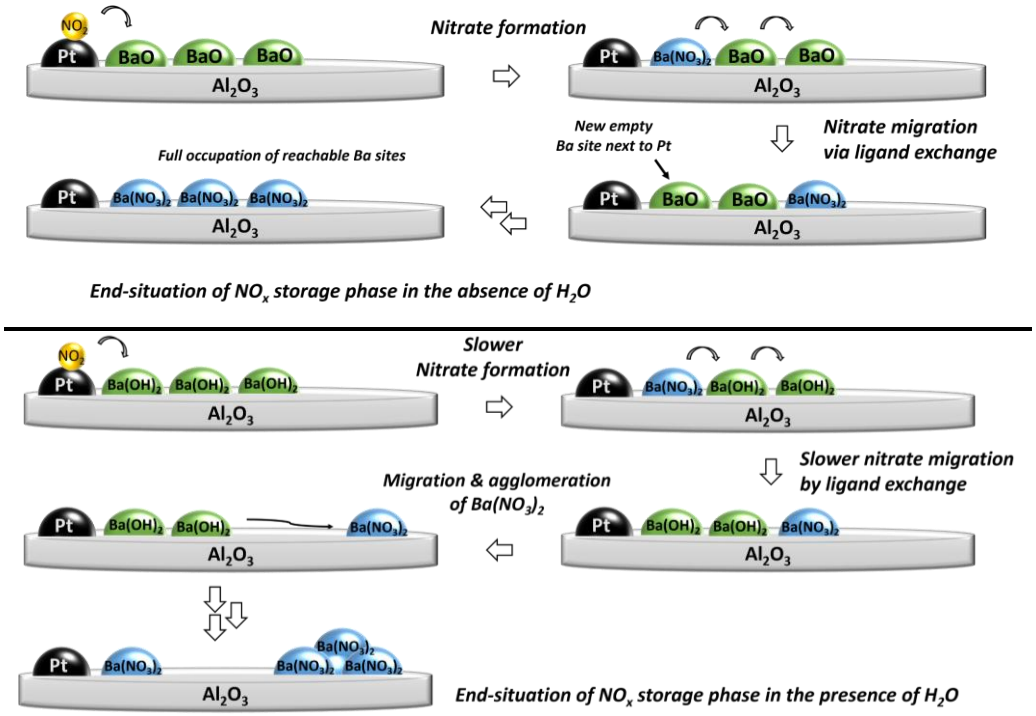

Fig. 7: NO_x storage mechanism under dry (above) and wet (below) conditions.

3.2.2 Water influence on NH_3 formation

The impact of H_2O on the nitrate reduction with H_2 to NH_3 during the second phase of the cycle is generally beneficial, according to literature, although variations in the actual influence of H_2O have been reported among different studies. Luo & Epling [29] appointed the rate-determining step in the reduction to be the spillover of hydrogen from Pt to $Ba(NO_3)_2$, and not the reverse spillover, namely of NO_x species from Ba to Pt sites. Mass transfer is, rather than the reaction itself, rate-determining in their vision. Reduction is slowest for $Ba(NO_3)_2$ farthest away from Pt. Those authors suggested that presence of H_2O improves this mass transfer by providing and stabilizing surface hydroxyl groups on the support [58].

Another explanation was offered by Zhu *et al.* [30], who stated, in the absence of H_2O, desorption of adsorbed NH_3 from Pt sites to be the rate-limiting step for nitrate reduction. Conversely, in the presence of H_2O, competitive adsorption between H_2O and NH_3 for the Pt sites occurs, resulting in increased yield of NH_3 [59].

The NH_3 selectivity of the stored nitrate reduction in the four Cases (Table 2) at a temperature of 150°C is reported in Fig. 8. The highest NH_3 selectivity of 82% is obtained after NO_x storage under dry conditions followed by reduction in presence of water (Case (II)). The presence of water during the whole cycle (Case (I)) with an NH_3 selectivity of 69% is second best. Reduction in absence of water leads to lower NH_3 selectivity's of 60% after NO_x storage in presence of water (Case (III)), and 55% in absence of water (Case (IV)).

These experiments confirm the beneficial effect of water observed in literature. NH_3 undergoes competitive adsorption with H_2O, enhancing its desorption instead of further reduction to N_2 [4,30]. The higher NH_3 selectivity in Case (III) compared to Case (IV) can be tentatively explained by the presence of some residual H_2O from the NO_x storage phase. Case (I) differs from Case (II) by the

presence of H_2O during the NO_x storage phase. The lower NH_3 selectivity of Case (I) can be explained by the different end-situations of the NO_x storage phase. A wet storage phase ends with agglomerates of $Ba(NO_3)_2$, at remote locations from Pt. $Ba(NO_3)_2$ species must undergo the reverse migration process to enable reduction of nitrate on Pt. This reverse migration proceeds better in the presence of H_2O hydroxylating the surface ensuring a swift supply of nitrate species to be reduced to NH_3. But still, this swift supply of stored nitrate to the Pt delays the reduction process and favors the consecutive reduction of nitrates by NH_3 towards N_2. In contrast, in Case (II), the storage phase does not end with $Ba(NO_3)_2$ agglomerates, leading to a smoother reduction process, followed by competitive adsorption with H_2O on the Pt sites, which favors the reduction towards NH_3 and not further towards N_2.

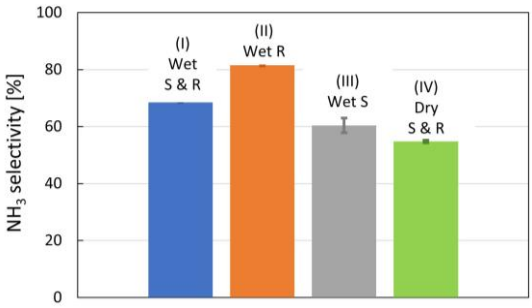

Fig. 8: NH_3 Selectivity [%] averaged over the reduction phase of the cycle at 150°C for Cases (I)-(IV) of Table 2. Three storage (S) and reduction (R) (250 s S/1800 s R) cycles performed at a GHSV of 60,000 h^{-1}.

The NH_3 selectivity averaged over the reduction phase of the cycle (Eq. 7) at different temperatures is presented in Fig. 9A for the four Cases. Fig. 9B depicts the maximum observed NH_3 concentration in the outlet gas stream at the investigated temperatures. In Cases (I), (II) and (IV), the NH_3 selectivity and peak concentration show a same trend with temperature. The maximum NH_3 selectivity and peak NH_3 concentration in the reactor outlet are attained within temperature range of 125-150°C. At higher temperatures, NH_3 selectivity and peak concentration decrease again. This can be explained by an enhanced reaction rate of the second step in the formation of N_2, namely the reduction of nitrates by NH_3, consuming NH_3 and lowering this way the NH_3 selectivity. At lower temperatures, desorption of NH_3 is too slow, also leading to reduction of nitrates by NH_3 [4]. Hence, the formation of NH_3 is favored in the intermediate temperature range of 125-150°C.

The NH_3 half peak width in function of temperature is presented in Fig. 9C. The peak width of Cases (I) and (II) does not vary with temperature. Hence, there is enough water present irrespective of temperature to favor NH_3 desorption. In Case (IV), the NH_3 half peak width is only determined by temperature, as no water is present in this case. As described above, difficult desorption can explain the high half peak width at low temperatures, while the increasing half peak width with higher temperatures can be attributed to the increasing reaction rate of the consecutive reaction of NH_3 with adsorbed nitrates.

Notably, Case (III), involving a wet storage and dry reduction phase, shows a completely different NH_3 selectivity, peak concentration and half peak width patterns in function of temperature (Fig. 9A, B and C). The NH_3 selectivity remains almost constant, while the peak concentration steadily decreases, and the half peak width increases with temperature. Here, agglomeration of $Ba(NO_3)_2$ during NO_x storage in presence of water causes a need of reverse migration of nitrate during the reduction phase towards the Pt. During reduction, water favoring reverse migration and NH_3 desorption is absent. The narrow NH_3 half peak width and high NH_3 peak leaving the reactor at the lowest temperature (75°C) point out that H_2O from the storage phase is still present in the beginning of the reduction phase and ensures competitive adsorption with formed NH_3. At higher temperatures, the adsorber-catalyst has less residual water and the benefit of competitive adsorption is lost. From there on, only $Ba(NO_3)_2$ agglomeration plays a role. Because the reverse motion is difficult without H_2O, there is a very slow supply of nitrates to Pt, favoring consecutive reaction towards N_2.

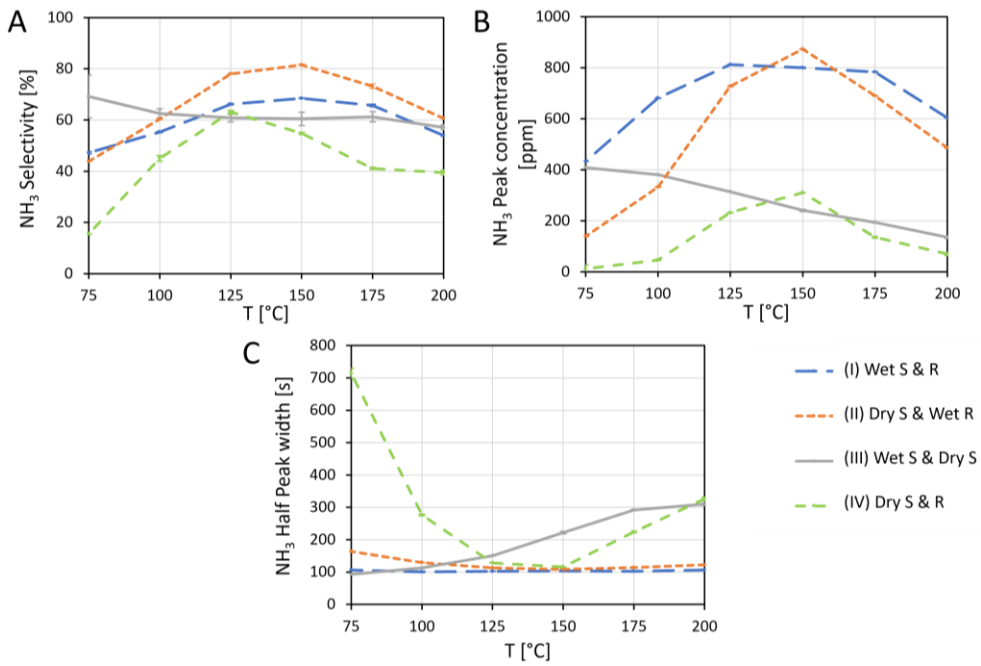

Fig. 9: A) NH_3 selectivity [%] averaged over the reduction phase of the cycle, B) NH_3 formation peak concentration in the outlet [ppm], and C) NH_3 concentration half peak width [s] against temperature in the range of 75-200°C for Cases (I)-(IV) of Table 2. Three storage (S)/reduction (R) (250 s S/1800 s R) cycles performed at each temperature at a GHSV of 60,000 h^{-1}. Error bars represent standard deviations. Legend applies to all figures.

TPD experiments were performed to validate these interpretations. A standard storage-reduction cycle at 75°C was performed, followed by programmed heating towards 450°C to desorb adsorbed N-species. The time evolution of the NH_3 outlet concentration during the reduction and TPD phase is represented in Fig. 10**.** Three different experiments are executed: an experiment without H_2O in storage, reduction, and TPD phase (Fig. 10A), an experiment without H_2O in storage, reduction, and TPD phase and with H_2 present during TPD (Fig. 10B), and an experiment with 4.2% H_2O present in storage, reduction, and TPD phase (Fig. 10C). The average NH_3 selectivity for each experiment is also noted in Fig. 10.

In the experiments in absence of water (Fig. 10A and B) at 75°C, no NH_3 was detected in the outlet until the TPD. NH_3 formed in the reduction phase remained adsorbed. However, in presence of water (Fig. 10C), NH_3 is already desorbing from the catalyst during reduction phase at a temperature as low as 75°C. It confirms the competitive adsorption between H_2O and NH_3 during reduction phase.

In the experiment with H_2 present during TPD (Fig. 10B), a higher NH_3 selectivity was obtained than in absence of H_2 (Fig. 10A), namely 75% versus 59%, respectively. This indicates that H_2 was able to reduce additional adsorbed nitrate species during the TPD phase, which were not reduced during the reduction phase at 75°C.

The molecular processes happening during the reduction phase under conditions without and with water in the entire cycle are sketched in Fig. 11 above and below, respectively. The dry reduction phase starts with the end-situation of the dry storage phase (Fig. 7). The trapped nitrates are located close by the Pt sites, and are primarily reduced by H_2, activated on Pt, towards NH_3. This nitrate reduction can be followed by reverse ligand exchange of nitrates, located further from Pt, with BaO sites at closer distance. Desorption of NH_3 can occur depending on temperature. Nitrates which subsequently reach Pt sites can be reduced by still-trapped NH_3 to form N_2.

The wet case (Fig. 12 below) has another starting point, as the end-situation of the storage phase is different from the dry case (Fig. 8). Initially, H_2 is activated by Pt and reduces the nearby nitrates to form NH_3. At this point, competitive adsorption on Pt between NH_3 and H_2O in the gas feed can occur, ensuring desorption of NH_3, independent of temperature. Later, remotely agglomerated $Ba(NO_3)_2$ needs to deliver nitrate species which migrate towards Pt by reverse ligand exchange. Approaching nitrates can in this case be reduced by H_2 towards NH_3.

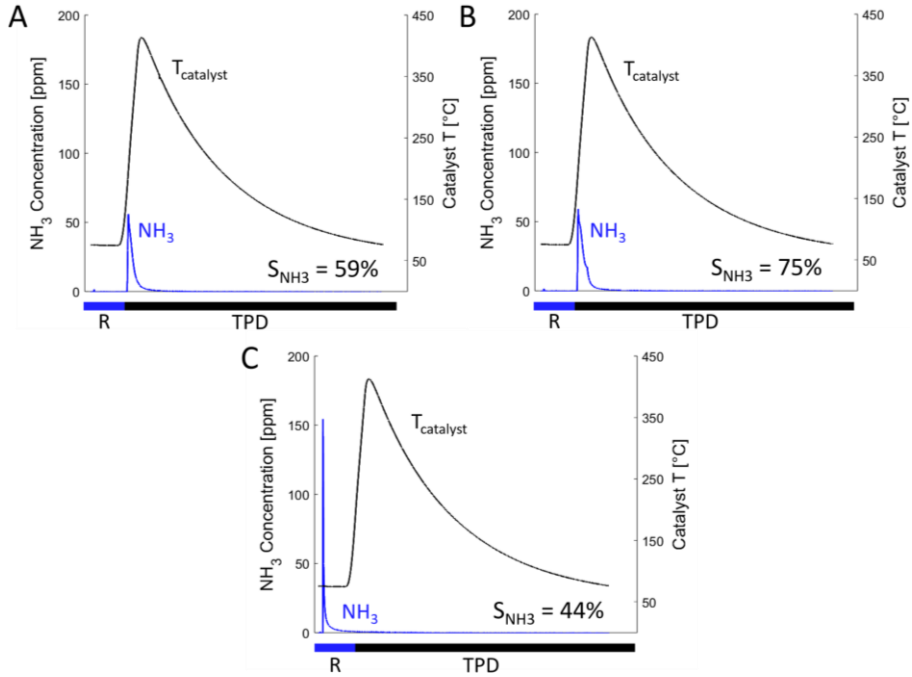

Fig. 10: Time evolution of NH_3 outlet concentration [ppm] (blue) and catalyst temperature [°C] (black) during reduction (R, blue bar) and temperature programmed desorption (TPD, black bar) phase, for three experiments: A) without H_2O during the entire test and without H_2 during TPD, B) without H_2O during the entire test and with H_2 during TPD, and C) with H_2O during the entire test and without H_2 during TPD. Catalyst (Pt/BaO/Al_2O_3 1/20/100) tested at 75°C for storage/reduction (250 s/1800 s) and heating to 450°C with holding time of 600 s in N_2 gas at a GHSV of 60,000 h^{-1}.

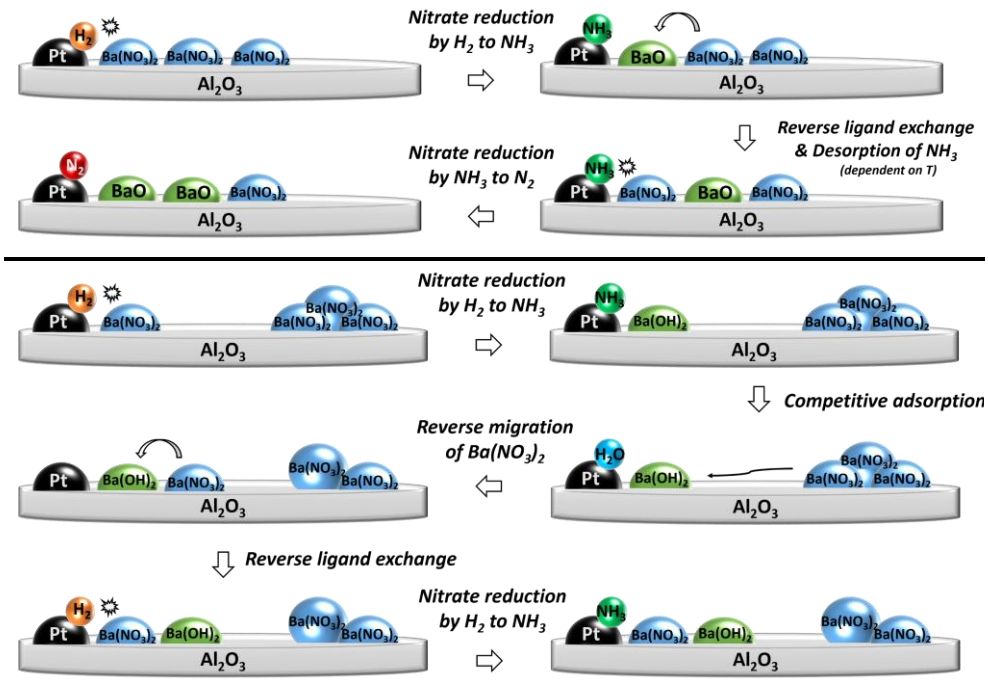

Fig. 11: Nitrate reduction towards NH_3 formation mechanism under dry (above) and wet (below) conditions.

3.3 Water concentration influence on storage and chemical reduction of stored NO_x

3.3.1 Water concentration influence on NO_x storage

In the previous section, the H_2O vapor content of the gases was fixed at 4.2%. Given its impact, the study was extended with a range of H_2O concentrations from 0.6% up to 14%. This range is based on the typical H_2O content in the exhaust of internal combustion processes [28,39] and corresponds to the boundary concentrations in our setup.

The dependency of the NO_x storage efficiency on the H_2O content of the gas mixture at three temperatures (75, 100 and 125°C) is shown in Fig. 12. The trend for each temperature is similar: a higher H_2O concentration lowers the NO_x storage efficiency. H_2O is expected to cover the adsorber-catalyst in a liquid-like layer [60]. The lower the temperature, the thicker the water layer. The NO molecule is poorly water soluble and may have difficulty to reach the active sites [61]. An H_2O concentration of 1-2% appears to be an optimum compromise between the detrimental effect of a water layer and the promoting role of H_2O in the storage mechanism already discussed.

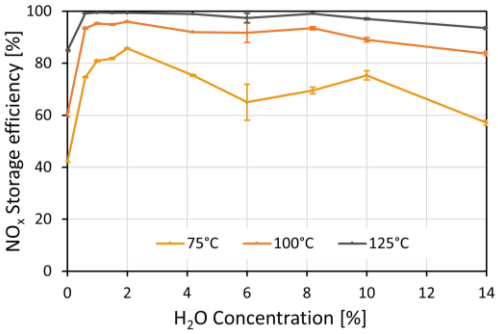

Fig. 12: NO_x Storage efficiency [%] during the storage phase of the cycle against H_2O concentration in the range of 0-14% at 75, 100, and 125°C. Pt/BaO/Al_2O_3 (1/20/100) is subjected three cycles of storage/reduction (250 s/1800 s) at a GHSV of 60,000 h^{-1}. Error bars represent standard deviations.

3.3.2 Water concentration influence on NH_3 formation

The influence of the H_2O concentration in the range 0 - 14% on the NH_3 selectivity at 150°C is shown in Fig. 13. The trends observed at this temperature are representative for other temperatures as well. Water at low concentration till 1.5% is beneficial and enhances the NH_3 selectivity to a maximum of 83%. More water vapor results in a drop of NH_3 selectivity to 29% at 14% H_2O. The beneficial role of H_2O is due to competitive adsorption of NH_3 and H_2O on the Pt sites. The detrimental effect can be explained by excessive coverage by H_2O of the catalyst surface [60]. A water layer counteracts the mobility of agglomerated nitrates as well as the nitrate reduction on the Pt sites. A possible additional consequence of this liquid-like surface layer is the solvation of formed NH_3, delaying desorption and causing the consecutive reaction towards N_2.

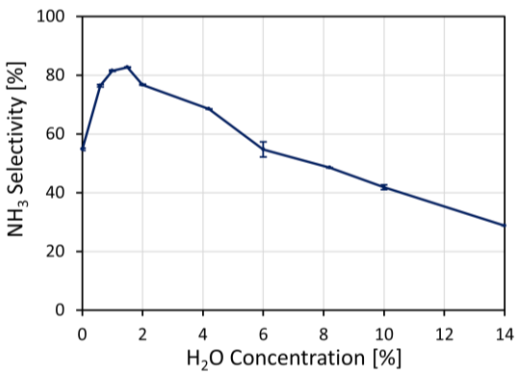

Fig. 13: NH_3 selectivity [%] averaged over the reduction phase of the cycle against H_2O concentration in the range of 0-14% at 150°C. Pt/BaO/Al_2O_3 (1/20/100) is subjected to three consecutive cycles of storage/reduction (250 s/1800 s) at a GHSV of 60,000 h^{-1}. Error bars represent standard deviations.

From the data of Fig. 12 and Fig. 13, it can be stated that the optimal water content in the LNT gas feed for the Pt/BaO/Al_2O_3 (1/20/100) catalyst is 1.5% H_2O. To gain maximum NH_3 selectivity, a future experiment should combine the optimal scenario in terms of H_2O, i.e., dry storage followed by wet reduction phase, and the optimal H_2O concentration of 1.5% H_2O.

The optimum is likely catalyst dependent. This comprehensive study on one specific catalyst formulation provides insight into properties that matter to LNT catalyst design targeting ammonia synthesis. The strength of the adsorption of H_2O on metal surfaces is metal dependent, and differences between the metals of interest in LNT research, Pt and Pd, are to be expected [60]. Furthermore, the support is of significant importance. When oxidized, H_2O can adsorb on metal oxide surfaces via H-bonding or by heterolytic splitting [62]. On one hand, surface area and porosity of the support are of importance. This can be understood based on the proposed mechanisms (Fig. 7 & Fig. 11): the thickness of the BaO and $Ba(OH)_2$ layers and of the agglomeration of $Ba(NO_3)_2$, and the availability of bare support surface area are dependent on the size of support surface. On the other hand, the surface chemistry is also crucial. TiO_2 and Al_2O_3 exhibits strong electrostatic interactions with H_2O by their cations Ti^{4+} and Al^{3+}, respectively. MgO is even more hydrophilic by the formation of $Mg(OH)_2$ with H_2O molecules [63]. The interaction mechanism of H_2O with ZrO_2 is less known [64]. Lackner *et al.* [64] demonstrated stronger H_2O adsorption on ZrO_2 than on Al_2O_3, while a separate study indicated more H_2O adsorption on ZrO_2 compared to TiO_2 [65].

4 Conclusions

This paper provides new insight in Lean NO_x Trap adsorptive and catalytic processes and ways to tune the formulation for NH_3 synthesis. Catalyst preparations with different supports and variation between noble metal reveal the strong impact of compositional parameters. Higher NH_3 selectivity's are obtained with Pt compared to Pd and bimetallic Pt-Pd combinations. γ-Al_2O_3 support outperforms TiO_2, ZrO_2 and MgO, which is mainly due to its high specific surface area and porosity. The nature of the support appeared to be important for spreading of the barium phase and preventing the platinum phase deposited first on the support, to become less accessible by coverage with the barium phase.

Water is found to play a key role in the NO_x adsorption – catalytic reduction cycle and insight into the beneficial role of water is essential for designing superior NO_x adsorbent – catalytic reduction formulations. The presence of water vapor has manifold benefits. During the NO_x storage phase, H_2O alters the adsorption chemistry in two ways: (I) it alters the speciation of Ba, viz the presence of $Ba(OH)_2$ instead of BaO, and (II) it facilitates migration and agglomeration of $Ba(NO_3)_2$ on the support surface. This latter affirms the better NO_x

storage in the presence of water during the storage phase. During the reduction phase, two effects of H_2O became apparent. (I) H_2O competes with generated NH_3 for adsorption on the Pt sites, facilitating desorption of NH_3. (II) Agglomeration of $Ba(NO_3)_2$ during the storage phase ensures surface diffusion and return of nitrates to the Pt sites to enable chemical reduction. Because of these two effects, the best combination for selective NH_3 formation on $Pt/BaO/Al_2O_3$ is a dry storage phase coupled with a wet reduction phase. But this may be support-dependent. If the water vapor content is to be kept constant throughout the cycle, the optimum H_2O concentration in the gas feed for $Pt/BaO/Al_2O_3$ is around 1.5%. Too much H_2O on the surface forms a liquid-like layer, hampering NO_x storage and stimulating the consecutive reaction towards N_2. Each catalyst formulation will have a different hydrophilic-hydrophobic balance and will have a different optimal H_2O concentration.

Acknowledgements

We gratefully acknowledge the organizing committee of PREPA13 for selecting our abstract. F.V.S. acknowledges Research Foundation Flanders (FWO) for granting an FWO-SB fellowship (No. 1S58723N). J.A.M. acknowledges the Flemish Government for long-term structural funding (Methusalem). This work was supported by the Industrial Research fund (IOF) (project No. C3/20/067). The graphical abstract has been designed using assets from Freepik.com.

References

[1] S. Matsumoto, Catalytic reduction of nitrogen oxides in automotive exhaust containing excess oxygen by NO x storage-reduction catalyst, Cattech. 4 (2000). https://doi.org/10.1023/A:1011951415060.

[2] N. Miyoshi, S. Matsumoto, K. Katoh, T. Tanaka, J. Harada, N. Takahashi, K. Yokota, M. Sugiura, K. Kasahara, Development of New Concept Three-Way Catalyst for Automotive Lean-Burn Engines, in: Journal of Engines, Michigan, 1995: pp. 1361–1370. https://doi.org/10.4271/950809.

[3] P. Granger, V.I. Parvulescu, Catalytic NOx abatement systems for mobile sources: From three-way to lean burn after-treatment technologies, 2011. https://doi.org/10.1021/cr100168g.

[4] L. Lietti, I. Nova, P. Forzatti, Role of ammonia in the reduction by hydrogen of NOx stored over Pt–Ba/Al2O3 lean NOx trap catalysts, J Catal. 257 (2008) 270–282. https://doi.org/10.1016/j.jcat.2008.05.005.

[5] R.D. Clayton, M.P. Harold, V. Balakotaiah, Performance Features of Pt/BaO lean NOx trap with hydrogen as reductant, AIChE Journal. 55 (2009) 687–700. https://doi.org/10.1002/aic.11710.

[6] A. Reihani, B. Corson, J.W. Hoard, G.B. Fisher, E. Smirnov, D. Roemer, J. Theis, C. Lambert, Rapidly Pulsed Reductants in Diesel NOx Reduction by Lean NOx Traps: Effects of Mixing Uniformity and Reductant Type, Source: SAE International Journal of Engines. 9 (2016) 1630–1641. https://doi.org/10.2307/26284928.

[7] P. Kočí, F. Plát, J. Štěpánek, M. Kubíček, M. Marek, Dynamics and selectivity of NOx reduction in NOx storage catalytic monolith, Catal Today. 137 (2008) 253–260. https://doi.org/10.1016/j.cattod.2007.11.023.

[8] S. Roy, A. Baiker, NO $_x$ Storage−Reduction Catalysis: From Mechanism and Materials Properties to Storage−Reduction Performance, Chem Rev. 109 (2009) 4054–4091. https://doi.org/10.1021/cr800496f.

[9] G. Liu, P.X. Gao, A review of NOx storage/reduction catalysts: Mechanism, materials and degradation studies, Catal Sci Technol. 1 (2011) 552–568. https://doi.org/10.1039/c1cy00007a.

[10] W.S. Epling, L.E. Campbell, A. Yezerets, N.W. Currier, J.E. Parks, Overview of the Fundamental Reactions and Degradation Mechanisms of NOx Storage/Reduction Catalysts, Catalysis Reviews. 46 (2004) 163–245. https://doi.org/10.1081/CR-200031932.

[11] W.P. Partridge, J.S. Choi, NH3 formation and utilization in regeneration of Pt/Ba/Al2O3 NOx storage-reduction catalyst with H2, Appl Catal B. 91 (2009) 144–151. https://doi.org/10.1016/j.apcatb.2009.05.017.

[12] J.S. Choi, W.P. Partridge, J.A. Pihl, M.Y. Kim, P. Kočí, C.S. Daw, Spatiotemporal distribution of NO x storage and impact on NH 3 and N 2O selectivities during lean/rich cycling of a Ba-based lean NO x trap catalyst, in: Catal Today, 2012: pp. 20–26. https://doi.org/10.1016/j.cattod.2011.11.007.

[13] L. Cumaranatunge, S.S. Mulla, A. Yezerets, N.W. Currier, W.N. Delgass, F.H. Ribeiro, Ammonia is a hydrogen carrier in the regeneration of Pt/BaO/Al2O3 NOx traps with H2, J Catal. 246 (2007) 29–34. https://doi.org/10.1016/j.jcat.2006.11.008.

[14] S. Hackenberg, M. Ranalli, Ammonia on a LNT: Avoid the Formation or Take Advantage of It, in: Control, Michigan, 2007. https://doi.org/10.4271/2007-01-1239.

[15] C. Depcik, D. Assanis, K. Bevan, A one-dimensional lean NOx trap model with a global kinetic mechanism that includes NH3 and N2O, International Journal of Engine Research. 9 (2008) 57–77. https://doi.org/10.1243/14680874JER01807.

[16] J.L. Sorrels, D.D. Randall, K.S. Schaffner, C. Richardson Fry, Chapter 2. Selective Catalytic Reduction, 2019.

[17] J. Parks, V. Prikhodko, Ammonia production and utilization in a hybrid LNT+SCR system, SAE Technical Papers. (2009). https://doi.org/10.4271/2009-01-2739.

[18] T. Wittka, B. Holderbaum, T. Maunula, M. Weissner, Development and Demonstration of LNT+SCR System for Passenger Car Diesel Applications, SAE Int J Engines. 7 (2014) 1269–1279. https://doi.org/10.4271/2014-01-1537.

[19] M. Cortés-Reyes, C. Herrera, M.Á. Larrubia, L.J. Alemany, Hybrid technology for DeNOxing by LNT-SCR system for efficient diesel emission control: Influence of operation parameters in H2O + CO2 atmosphere, Catalysts. 10 (2020). https://doi.org/10.3390/catal10020228.

[20] L. Hollevoet, F. Jardali, Y. Gorbanev, J. Creel, A. Bogaerts, J.A. Martens, Towards Green Ammonia Synthesis through Plasma-Driven Nitrogen Oxidation and Catalytic Reduction, Angewandte Chemie International Edition. 59 (2020) 23825–23829. https://doi.org/10.1002/anie.202011676.

[21] L. Hollevoet, E. Vervloessem, Y. Gorbanev, A. Nikiforov, N. De Geyter, A. Bogaerts, J.A. Martens, Energy-Efficient Small-Scale Ammonia Synthesis Process with Plasma-Enabled Nitrogen Oxidation and Catalytic Reduction of Adsorbed NOx, ChemSusChem. 15 (2022). https://doi.org/10.1002/cssc.202102526.

[22] C.D. DiGiulio, J.A. Pihl, J.-S. Choi, J.E. Parks, M.J. Lance, T.J. Toops, M.D. Amiridis, NH3 formation over a lean NOX trap (LNT) system: Effects of lean/rich cycle timing and temperature, Appl Catal B. 147 (2014) 698–710. https://doi.org/10.1016/j.apcatb.2013.09.012.

[23] B.M. Shakya, M.P. Harold, V. Balakotaiah, Effect of cycle time on NH3 generation on low Pt dispersion Pt/BaO/Al2O3 catalysts: Experiments and crystallite-scale modeling, Chemical Engineering Journal. 230 (2013) 584–594. https://doi.org/10.1016/j.cej.2013.06.109.

[24] P. Forzatti, L. Lietti, N. Gabrielli, A kinetic study of the reduction of NOx stored on Pt-Ba/Al2O3 catalyst, Appl Catal B. 99 (2010) 145–155. https://doi.org/10.1016/j.apcatb.2010.06.011.

[25] J.M. García-Cortés, J. Pérez-Ramírez, M.J. Illán-Gómez, F. Kapteijn, J.A. Moulijn, C. Salinas-Martínez De Lecea, Comparative study of Pt-based catalysts on different supports in the low-temperature de-NO x-SCR with propene, 2001.

[26] R. Burch, P.J. Millington, Selective reduction of NO x by hydrocarbons in excess oxygen by alumina-and silica-supported catalysts, 1996.

[27] K. ichi Shimizu, Y. Saito, T. Nobukawa, N. Miyoshi, A. Satsuma, Effect of supports on formation and reduction rate of stored nitrates on NSR catalysts as investigated by in situ FT/IR, Catal Today. 139 (2008) 24–28. https://doi.org/10.1016/j.cattod.2008.08.004.

[28] Hannu Jääskeläinen, Diesel Exhaust Gas, DieselNet. (2020). https://dieselnet.com/tech/diesel_exh.php (accessed August 20, 2023).

[29] J.-Y. Luo, W.S. Epling, New insights into the promoting effect of H2O on a model Pt/Ba/Al2O3 NSR catalyst, Appl Catal B. 97 (2010) 236–247. https://doi.org/10.1016/j.apcatb.2010.04.007.

[30] J. Zhu, J. Wang, J. Wang, L. Lv, X. Wang, M. Shen, New Insights into the N_2 O Formation Mechanism over Pt-BaO/Al_2O_3 Model Catalysts Using H_2 As a Reductant, Environ Sci Technol. 49 (2015) 504–512. https://doi.org/10.1021/es5046106.

[31] P. Forzatti, L. Castoldi, L. Lietti, I. Nova, E. Tronconi, Identification of the reaction networks of the NOx storage/reduction in Lean NOx Trap systems, in: P. Granger, V. Pârvulescu (Eds.), Past and Present in DeNOx Catalysis, 1st ed., Elsevier Science, 2007: pp. 175–208.

[32] L. Lietti, P. Forzatti, I. Nova, E. Tronconi, NOx storage reduction over Pt-Ba/γ -Al2O3 catalyst, J Catal. 204 (2001) 175–191. https://doi.org/10.1006/jcat.2001.3370.

[33] M. De Prins, E. Verheyen, A. Hoffmann, G. Vanbutsele, S.P. Sree, S. Kerkhofs, L. Van Tendeloo, F.W. Schütze, J. Martens, Structural parameters governing low temperature activity of small pore copper zeolites in NH3-SCR, J Catal. 390 (2020) 224–236. https://doi.org/10.1016/j.jcat.2020.08.003.

[34] D. Mráček, P. Kočí, J.S. Choi, W.P. Partridge, New operation strategy for driving the selectivity of NOx reduction to N2, NH3 or N2O during lean/rich cycling of a lean NOx trap catalyst, Appl Catal B. 182 (2016) 109–114. https://doi.org/10.1016/j.apcatb.2015.09.002.

[35] A. Benato, A. Macor, A. Rossetti, Biogas Engine Emissions: Standards and On-Site Measurements, in: Energy Procedia, Elsevier Ltd, 2017: pp. 398–405. https://doi.org/10.1016/j.egypro.2017.08.278.

[36] M. Ilbas, I. Yilmaz, Y. Kaplan, Investigations of hydrogen and hydrogen-hydrocarbon composite fuel combustion and NOx emission characteristics in a model combustor, Int J Hydrogen Energy. 30 (2005) 1139–1147. https://doi.org/10.1016/j.ijhydene.2004.10.016.

[37] European Commission, Large Volume Inorganic Chemicals - Ammonia, Acids and Fertilisers, 2007. https://eippcb.jrc.ec.europa.eu/reference/large-volume-inorganic-chemicals-ammonia-acids-and-fertilisers (accessed October 30, 2023).

[38] Manufacturers of Emission Controls Association (MECA), Emission Control Technology for Stationary Internal Combustion Engines, Arlington, 2015. www.meca.org.

[39] P. Avlla, C. Barthelemy, A. Bahamonde, J. Blanco, Catalyst for NOx removal in nitric-acid plant: Gaseous Effluents, Atmos Environ. 27 (1993) 443–447.

[40] R.D. Clayton, M.P. Harold, V. Balakotaiah, Performance Features of Pt/BaO lean NOx trap with hydrogen as reductant, AIChE Journal. 55 (2009) 687–700. https://doi.org/10.1002/aic.11710.

[41] L. Hollevoet, E. Vervloessem, Y. Gorbanev, A. Nikiforov, N. de Geyter, A. Bogaerts, J.A. Martens, Energy-Efficient Small-Scale Ammonia Synthesis Process with Plasma-enabled Nitrogen Oxidation and Catalytic Reduction of Adsorbed NOx, ChemSusChem. (2022). https://doi.org/10.1002/cssc.202102526.

[42] D. Roizard, Antoine Equation, in: Encyclopedia of Membranes, Springer Berlin Heidelberg, 2014: pp. 1–3. https://doi.org/10.1007/978-3-642-40872-4_26-1.

[43] J.P. Breen, R. Burch, N. Lingaiah, An investigation of catalysts for the on board synthesis of NH3. A possible route to low temperature NOx reduction for lean-burn engines, Catal Letters. 79 (2002) 171–174. https://doi.org/10.1023/A:1015368627496.

[44] E.C. Adams, M. Skoglundh, P. Gabrielsson, M. Laurell, P.A. Carlsson, Ammonia formation over Pd/Al2O3 modified with cerium and barium, Catal Today. 267 (2016) 210–216. https://doi.org/10.1016/j.cattod.2016.01.012.

[45] J.A. Onrubia-Calvo, B. Pereda-Ayo, A. Caravaca, U. De-La-Torre, P. Vernoux, J.R. González-Velasco, Tailoring perovskite surface composition to design efficient lean NOx trap Pd–La1-xAxCoO3/Al2O3-type catalysts (with A = Sr or Ba), Appl Catal B. 266 (2020). https://doi.org/10.1016/j.apcatb.2020.118628.

[46] T.C. Watling, P.D. Bolton, D. Swallow, Comparison of different kinetic models for NOX storage on a lean NOX trap, Canadian Journal of Chemical Engineering. 92 (2014) 1506–1516. https://doi.org/10.1002/cjce.22015.

[47] Y. Zhang, Y. Zhou, J. Shi, S. Zhou, X. Sheng, Z. Zhang, S. Xiang, Comparative study of bimetallic Pt-Sn catalysts supported on different supports for propane dehydrogenation, J Mol Catal A Chem. 381 (2014) 138–147. https://doi.org/10.1016/j.molcata.2013.10.007.

[48] C. Sedlmair, K. Seshan, A. Jentys, J.A. Lercher, Elementary steps of NOx adsorption and surface reaction on a commercial storage-reduction catalyst, J Catal. 214 (2003) 308–316. https://doi.org/10.1016/S0021-9517(02)00085-4.

[49] S.S. Chaugule, A. Yezerets, N.W. Currier, F.H. Ribeiro, W.N. Delgass, "Fast" NOx storage on Pt/BaO/γ-Al2O3 Lean NOx Traps with NO2 + O2 and NO + O2: Effects of Pt, Ba loading, in: Catal Today, 2010: pp. 291–303. https://doi.org/10.1016/j.cattod.2010.02.024.

[50] L. Chen, W. Sun, Z. Xu, M. Hao, B. Li, X. Liu, J. Ma, L. Wang, C. Li, W. Wang, Ultrafine Cu nanoparticles decorated porous TiO2 for high-efficient electrocatalytic reduction of NO to synthesize NH3, Ceram Int. 48 (2022) 21151–21161. https://doi.org/10.1016/j.ceramint.2022.04.006.

[51] S. Morandi, F. Prinetto, G. Ghiotti, L. Castoldi, L. Lietti, P. Forzatti, M. Daturi, V. Blasin-Aubé, The influence of CO2 and H2O on the storage properties of Pt-Ba/Al2O3 LNT catalyst studied by FT-IR spectroscopy and transient microreactor experiments, Catal Today. 231 (2014) 116–124. https://doi.org/10.1016/j.cattod.2013.12.036.

[52] G.M. Habashy, G.A. Kolta, Thermal decomposition of the hydrates of barium hydroxide, Journal of Inorganic and Nuclear Chemistry. 34 (1972) 57–67. https://doi.org/10.1016/0022-1902(72)80361-0.

[53] L. Lietti, P. Forzatti, I. Nova, E. Tronconi, NOx storage reduction over Pt-Ba/γ -Al2O3 catalyst, J Catal. 204 (2001) 175–191. https://doi.org/10.1006/jcat.2001.3370.

[54] N. Le Phuc, X. Courtois, F. Can, S. Berland, P. Marecot, D. Duprez, A study of the ammonia selectivity on Pt/BaO/Al2O3 model catalyst during the NOx storage and reduction process, Catal Today. (2011). https://doi.org/10.1016/j.cattod.2010.10.080ï.

[55] J. Szanyi, J.H. Kwak, D.H. Kim, X. Wang, R. Chimentao, J. Hanson, W.S. Epling, C.H.F. Peden, Water-induced morphology changes in BaO/γ-Al2O3 NOx storage materials: An FTIR, TPD, and time-resolved synchrotron XRD study, Journal of Physical Chemistry C. 111 (2007) 4678–4687. https://doi.org/10.1021/jp067932v.

[56] D.H. Kim, K. Mudiyanselage, J. Szanyi, J.C. Hanson, C.H.F. Peden, Effect of H2O on the morphological changes of KNO3 formed on K2O/Al2O3 NOx storage materials: Fourier transform infrared and time-resolved X-ray diffraction studies, Journal of Physical Chemistry C. 118 (2014) 4189–4197. https://doi.org/10.1021/jp410816r.

[57] D. Mei, Q. Ge, J.H. Kwak, D.H. Kim, C. Verrier, J. Szanyi, C.H.F. Peden, Characterization of surface and bulk nitrates of γ-Al 2O 3-supported alkaline earth oxides using density functional theory, Physical Chemistry Chemical Physics. 11 (2009) 3380–3389. https://doi.org/10.1039/b819347a.

[58] L. Castoldi, L. Lietti, P. Forzatti, S. Morandi, G. Ghiotti, F. Vindigni, The NOx storage-reduction on PtK/Al2O3 Lean NOx Trap catalyst, J Catal. 276 (2010) 335–350. https://doi.org/10.1016/j.jcat.2010.09.026.

[59] X. Zhao, X. Zhang, Y. Xu, Y. Liu, X. Wang, Q. Yu, The effect of H2O on the H2-SCR of NOx over Pt/HZSM-5, J Mol Catal A Chem. 400 (2015) 147–153. https://doi.org/10.1016/j.molcata.2015.02.013.

[60] J. Carrasco, A. Hodgson, A. Michaelides, A molecular perspective of water at metal interfaces, Nat Mater. 11 (2012) 667–674. https://doi.org/10.1038/nmat3354.

[61] S. Budavari, The Merck index : an encyclopedia of chemicals, drugs, and biologicals, 15th ed., Royal Society of Chemistry, 1996.

[62] M. Henderson, The interaction of water with solid surfaces: fundamental aspects revisited, Surf Sci Rep. 46 (2002) 1–308. https://doi.org/10.1016/S0167-5729(01)00020-6.

[63] M. Takeuchi, R. Kurosawa, J. Ryu, Vibrational spectroscopic evaluation of hydrophilic or hydrophobic properties of oxide surfaces, Journal of Raman Spectroscopy. 53 (2022) 1793–1804. https://doi.org/10.1002/jrs.6380.

[64] P. Lackner, J. Hulva, E.M. Köck, W. Mayr-Schmölzer, J.I.J. Choi, S. Penner, U. Diebold, F. Mittendorfer, J. Redinger, B. Klötzer, G.S. Parkinson, M. Schmid, Water adsorption at zirconia: From the ZrO2(111)/Pt3Zr(0001) model system to powder samples, J Mater Chem A Mater. 6 (2018) 17587–17601. https://doi.org/10.1039/c8ta04137g.

[65] A. Ignatchenko, D.G. Nealon, R. Dushane, K. Humphries, Interaction of water with titania and zirconia surfaces, J Mol Catal A Chem. 256 (2006) 57–74. https://doi.org/10.1016/j.molcata.2006.04.031.